Redefining the Directional-Hemispherical Reflectance and Transmittance of Needle- Shaped Leaves to Address Issues in Their Existing Measurement Methods

Article *in* Photogrammetric Engineering and Remote Sensing · October 2020

DOI: 10.14358/PERS.86.10.1

CITATIONS
0

READS
201

5 authors, including:

Jun Wang
Fujian Normal University
7 PUBLICATIONS **16** CITATIONS
SEE PROFILE

Lian Feng
Southern University of Science and Technology
112 PUBLICATIONS **3,181** CITATIONS
SEE PROFILE

Jianhui Xu
Guangzhou Institute of Geography
41 PUBLICATIONS **288** CITATIONS
SEE PROFILE

Redefining the Directional-Hemispherical Reflectance and Transmittance of Needle-Shaped Leaves to Address Issues in Their Existing Measurement Methods

Jun Wang, Jing M. Chen, Lian Feng, Jianhui Xu, and Feifei Zhang

Abstract

The directional-hemispherical reflectance and transmittance of needle-shaped leaves are redefined in this study. We suggest that the reflected and transmitted radiation of a leaf should be distinguished by the illuminated and shaded leaf surfaces rather than the usual separation of the two hemispheres by a plane perpendicular to the incoming radiation. Through theoretical analysis, we found that needle directional-hemispherical reflectance and transmittance measured by two existing techniques, namely Daughtry's method and Harron's method, could be significantly biased. This finding was proved by ray-tracing simulations intuitively as well as by inversions of the PROSPECT *model indirectly. We propose the following requirements for needle spectral measurement in an integrating sphere: needles should be fully exposed to the light source, the interfusion of reflected and transmitted radiation on convex needle surfaces should be avoided, and multiple scattering of radiation among needles should be minimized.*

Introduction

Needle-leaved plants represent a significant fraction of natural terrestrial ecosystems. For example, the boreal forest, the second-largest needle-leaf-dominated forest biome in the world (Astrup *et al.* 2018), covers ~50% of the North American boreal zone (Brandt *et al.* 2013) and nearly one-third of the Earth's forest area (MacDicken *et al.* 2015). Thus, monitoring the temporal and spatial variation of needle-leaved plants is in the interest of studies of global change. The advent of spectroscopy and remote sensing has made such monitoring more efficient, convenient, and intuitive. The accuracy of relevant results, as well as the validity of corresponding conclusions, heavily depends on the fidelity of collected leaf spectra, which are the basic data required for retrieving leaf biochemical and biophysical traits.

An integrating sphere is a device commonly used in the remote-sensing community for leaf spectral measurements, due to its solid theoretical basis (Jacquez and Kuppenheim 1955; Miller and Sant 1958). It is a highly reflective cavity in appearance, with several holes or ports reserved for attaching samples, holding a light source or a white reference. When connected with a spectrometer, signals within the sphere can be captured so as to produce a reflectance, transmittance, or absorption curve. In most circumstances, the sample port of an integrating sphere can be completely covered by broad leaves, whose reflected and transmitted radiation can be clearly separated in this way (Figure 1a). However, needle-shaped leaves have distinct morphological characteristics. They are always too narrow to completely cover the sample port of an integrating sphere. Existing techniques, namely Daughtry's method and Harron's method, measure the directional-hemispherical reflectance (DHR) and transmittance (DHT) of needle-shaped leaves by putting an array of needle samples into a sample holder, which has to be no smaller than the sample port to be attached (the sample holder is also called a *carrier* in other studies). As already mentioned, an integrating sphere only

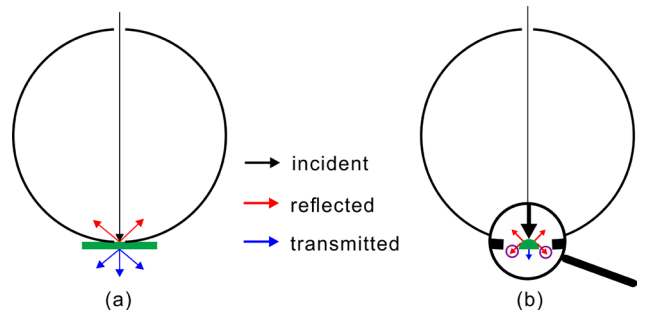

Figure 1. Spectral measurements of (a) a broad leaf and (b) a needle with an integrating sphere. A magnifier is used to zoom in on the needle in (b). The needle, with convex surfaces, is narrower than the sample port of the integrating sphere. Part of the reflected radiation (pointed out by purple circles) goes in the forward direction away from the light source and is mixed with transmitted radiation. As a result, it is misclassified.

Jun Wang and Lian Feng are with the School of Environmental Science and Technology, Southern University of Science and Technology, Shenzhen, China (fengl@sustech.edu.cn).

Jing M. Chen is with the International Institute for Earth System Science, Nanjing University, Nanjing, China (jing.chen@utoronto.ca).

Jianhui Xu is with the Key Laboratory of Guangdong for Utilization of Remote Sensing and Geographical Information System, Guangdong Open Laboratory of Geospatial Information Technology and Application, Guangzhou Institute of Geography, Guangzhou, China; and the Southern Marine Science and Engineering Guangdong Laboratory, Guangzhou, China.

Feifei Zhang is with the Department of Computer Science, Guangdong University of Education, Guangzhou, China.

Photogrammetric Engineering & Remote Sensing
Vol. 86, No. 10, October 2020, pp. 19–491.
0099-1112/20/19–491

doi: 10.14358/PERS.86.10.1

captures signals within the sphere; therefore, the two faces of the sample holder serve as the *de facto* reference plane for needles to distinguish reflected and transmitted radiation. The validity of such methods needs to be examined, as some radiation can be hard to define. For example, the radiation indicated by purple circles in Figure 1b is reflected at the needle surface but goes in the forward direction away from the light source and is not captured by the integrating sphere. As a result, it will be regarded as transmitted radiation. This phenomenon pushed us to review the definitions of DHR and DHT for needle-shaped leaves. However, we failed to find a clear definition in the existing literature. In order to solve the problem, it is necessary to define the DHR and DHT for needle-shaped leaves.

The DHR and DHT of a unit surface already have clear definitions (Schaepman-Strub *et al.* 2006). However, leaves are more than just flat surfaces, as they can also be thick objects. When a ray hits a surface without thickness, it will be either reflected from the surface or refracted after penetrating through the surface, following physical laws described by Fresnel or Snell's equations; but when a leaf has a certain thickness, the ray penetrating through the leaf surface will undergo an additional radiative transfer process by interacting with the interior of the leaf. In this case, the reflectance from the surface contains two parts: the surface reflection and the internal scattering (Jacquemoud and Ustin 2008). In most circumstances, a lamina bifacial leaf has upper (facing incoming radiation) and lower (shaded) surfaces on which reflectance and transmittance can be defined. In these circumstances, the definitions of DHR and DHT for a unit surface can be applied directly to flat leaves such as broad leaves. But needle-shaped leaves are quite special and different in their morphological characteristics. With comparable width and thickness, needles could have many sides or circular or semicircular cross-sectional shapes, which do not have clear upper and lower surfaces. This raises an important issue for spectral measurements of needle reflectance and transmittance: how to distinguish reflected and transmitted radiation for needle-shaped leaves? This issue can be addressed faithfully by extending the DHR and DHT from unit surfaces to needles.

The goal of this article is to investigate the methods to separate reflected and transmitted radiation from needle-shaped leaves, based on which the DHR and DHT of needle-shaped leaves can be defined. The potential drawbacks of two existing techniques for measurements of needle DHR and DHT are also analyzed to demonstrate the importance of this separation. The specific objectives of this article are to demonstrate that the reflected and transmitted radiation of a leaf should be distinguished by the illuminated and shaded leaf surfaces, and to investigate the requirements for measuring needle reflectance and transmittance.

Theory

Defining the DHR and DHT for Needle-Shaped Leaves

In this section, a needle with a semicircular cylindrical shape is shown as an example (Table 1). The definition given in the present study can also be applied to needles of other shapes. The needle has two degrees of freedom to describe its angular position, according to Chen and Black (1992): the longitudinal axis of the cylinder and the normal to the surface of some reference plane associated with the leaf. Only the cross-sectional views of the needle are displayed. All directions in three-dimensional space are projected into the cross-sectional plane.

Identifying the Reflected and Transmitted Radiation of a Needle by the Illuminated and Shaded Leaf Surfaces

The DHR of a unit surface is defined as the ratio of the radiant flux for light reflected by a unit surface area into the view hemisphere to the illumination radiant flux (Figure 2a; Schaepman-Strub *et al.* 2006). When the definition applies to a broad surface, no matter flat or rough, the total reflected radiant flux integrated over the whole illuminated face should be

Table 1. Simulating Daughtry's, Harron's and Defined reflectance and transmittance for two different needle shapes when light strike on two different sides of the needles.

Needle shape	Semicircular Needle		Regular Triangular Needle	
	Convex Side	Flat Side	Convex Side	Flat Side
Daughtry's	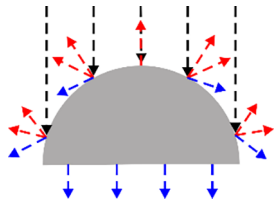	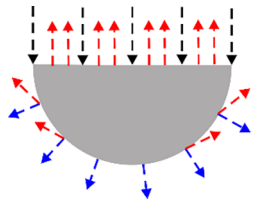	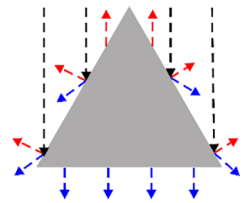	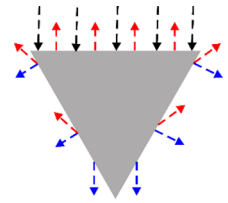
Harron's	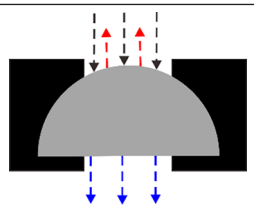	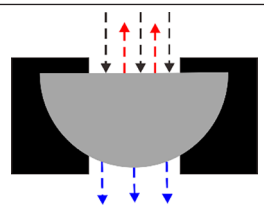	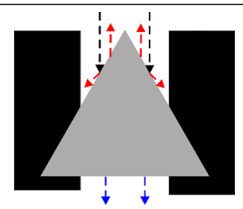	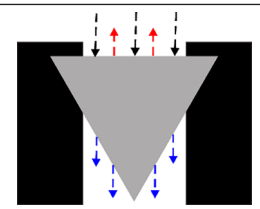
Defined	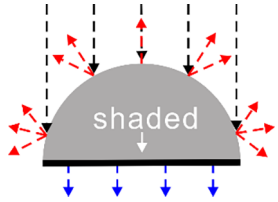	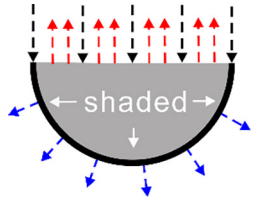	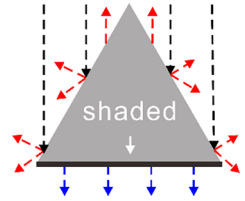	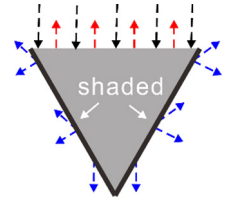

Incident radiation Reflected radiation Transmitted radiation

used instead (Figure 2b). Therefore, it can be inferred that the reflected and transmitted radiation of a broad surface should be distinguished by the illuminated and shaded faces. Similarly, the surface of a thick object such as a leaf (including but not limited to needles) can always be split into an illuminated part and a shaded part when exposed to collimated light, and the reflected and transmitted radiation can be separated by these two types of leaf surfaces (Figure 2c). All reflections happening at the leaf surface illuminated by the direct light (Figure 2c), regardless of their directions, contribute to the reflectance. The total reflectance also includes internally scattered radiation escaping from the illuminated side of the needle. The radiation escaping from the leaf interior via the shaded side of the needle is included in transmittance. It should be noted that the method proposed here to separate reflected and transmitted radiation is a generalized method which is also applicable to broad leaves. The shaded surface of a broad leaf includes the edges, which are always neglected in spectral measurements since little radiation comes out from this part of the leaf surface if the illuminated leaf surface is large enough (for example, as large as the sample port of an integrating sphere).

The Needle Being Measured Must Be Fully Illuminated

Although the reflectance and transmittance of a broad leaf may vary from one position to another due to the primary and secondary veins or due to surface roughness, they have been assumed to be quasi-identical across the whole leaf face, and the averaged values at several different points absent the primary veins are practically used in remote-sensing studies (e.g., Qiu *et al.* 2018). Therefore, broad leaves do not need to be fully illuminated in spectral measurements. In contrast, needle-shaped leaves are usually thick and narrow, and their leaf sides form a closed surface, not necessarily parallel or quasi-parallel. The reflectance and transmittance of a needle may change significantly when the needle is illuminated by collimated light in different directions (FIgures 3 and 11). Thus a needle being measured must be fully illuminated (Figure 3b)—i.e., when the projected area of the needle (PAN) on a plane perpendicular to the incident direction is equal to the projected area of the needle's illuminated surface (PAI).

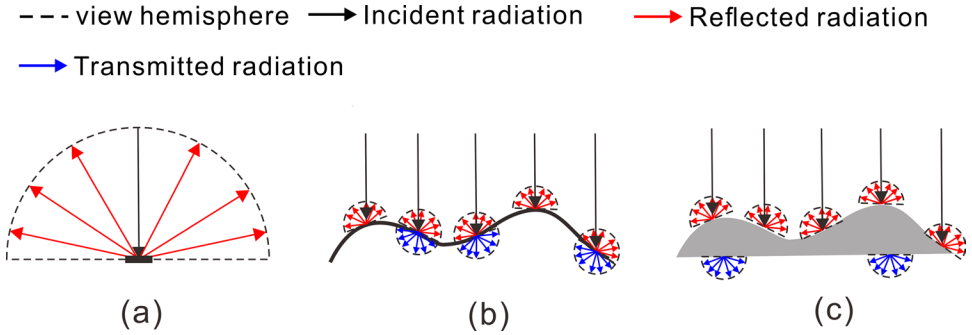

Figure 2. Extending the directional-hemispherical reflectance (DHR) for (a) a unit surface to (b) a broad surface and finally (c) a thick object. The mutual shadowing created by the surface has been neglected.

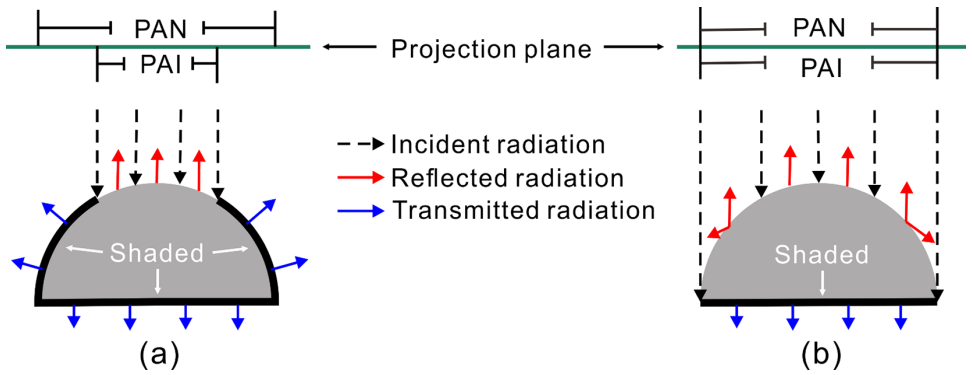

Figure 3. Illustrations of (a) partial and (b) full illumination of a needle. The needle surface is illuminated by collimated light in the same direction. The shaded leaf surfaces are highlighted by the thick black lines. PAN is the projected area of the needle on a plane perpendicular to the incident direction (green lines). PAI is the projected area of the needle's illuminated surface on a plane perpendicular to the incident direction. When PAN equals PAI, the needle is fully illuminated.

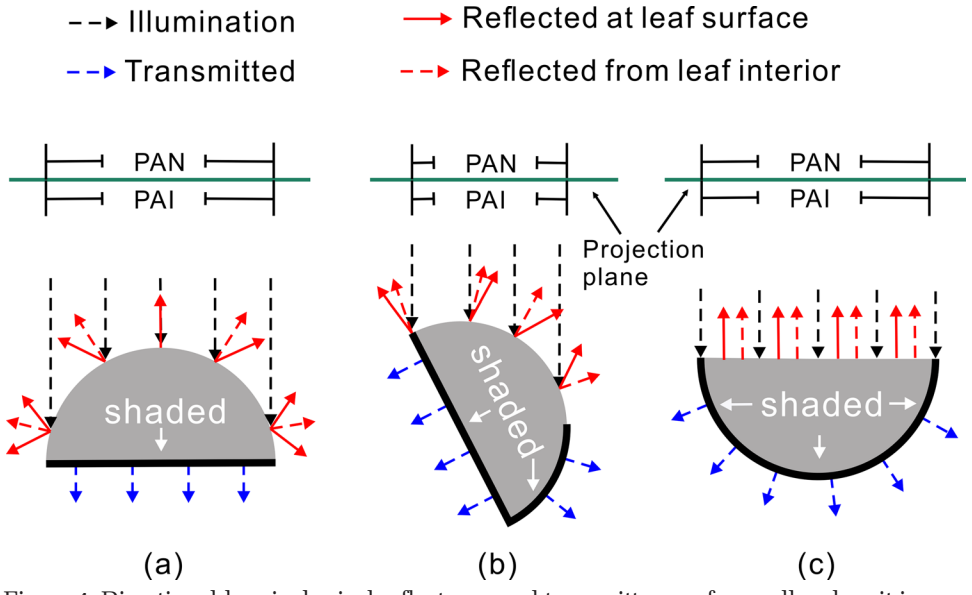

Figure 4. Directional-hemispherical reflectance and transmittance of a needle when it is fully illuminated by collimated light from different directions. The needle has a semicircular cross section (gray areas). PAN is the projected area of the needle on a plane perpendicular to the incident direction (green solid lines). The reflected and transmitted radiations are identified by the illuminated and shaded leaf surfaces. Note that in (a) and (b) the reflected radiation travels downward, crossing the horizontal plane. The shaded leaf surfaces are highlighted by thick black lines. All reflections happening at the leaf surface illuminated by direct light, regardless of their direction, contribute to the reflectance (red solid arrows). The total reflectance also includes internally scattered radiation escaping from the illuminated side of the needle (red dotted arrows). The radiation escaping from the leaf interior through the shaded side of the needle is included in the transmittance (blue dotted arrows).

Combined with the two points already mentioned, the DHR (DHT) of a needle is defined as the ratio of the total radiant flux reflected at or escaping from the illuminated surface (the internally scattered radiant flux escaping from the shaded surface) to the illumination radiant flux, when the needle is fully exposed to collimated light (Figure 4). The DHR and DHT of a needle may change with the illumination direction (Figures 4 and 11), and this change could be very large, since the needle morphology determines the distribution of incident angles—which is important for both the specular reflection at the needle surface and the diffuse scattering within the leaf tissues (McClendon 1984; Grant, Daughtry and Vanderbilt 1993). Therefore, the uncertainties caused by the illumination direction should be minimized, and it is strongly recommended to measure the DHR and DHT when the PAN is maximum and the illuminated leaf surface area is minimum (i.e., Figure 4c), which ensures a maximum probability of incidences happening at near-normal angles so that more light can enter into the needle. However, in some scenarios, such as simulating canopy reflectance by a geometrical-optical model, where needles are illuminated by light from various directions, it is better to average the DHR and DHT over different illumination angles.

Potential Drawbacks of Existing Techniques for Needle DHR and DHT Measurements

According to the review by Yáñez-Rausell *et al.* (2014), there are three main approaches to measuring DHR or DHT of needle-shaped leaves: Hosgood's (Hosgood *et al.* 1995), Harron's (Harron 2002), and Daughtry's method (Daughtry, Biehl and Ranson 1989). The first approach measures the infinite reflectance of a needle stack contained in a glass cuvette by putting the cuvette against the sample port of an integrating sphere, and therefore it is not a focus of this article. The other two approaches use a sample holder instead of a glass cuvette to expose a mat of needles to the sample port, and in this way the averaged DHR and DHT of a single needle can be measured. This section will make a brief introduction to the two existing methods for DHR and DHT measurement and analyze their strengths and limitations. There are other integrating-sphere-based methods to measure the reflectance and transmittance of needlelike leaves, such as double-integrating-sphere systems (Pickering *et al.* 1992; Pickering *et al.* 1993; Potůková *et al.* 2016; Mõttus, Hovi and Rautiainen 2017). The sample holders used in these methods are similar to that used in Daughtry's method; therefore, we regard them the same as Daughtry's method.

Daughtry's Method

The method proposed by Daughtry *et al.* (1989) measures the DHR and DHT by placing a mat of needles on tape (Figure 5) against the sample port of an integrating sphere. The key process of this method is to determine the gap fraction (GF) between needles, which was originally addressed by a painting technique with two-series measurements. However, the painting of each needle sample is labor-intensive and time-consuming, and therefore several studies (e.g., Middleton *et al.* 1996; Mesarch *et al.* 1999; Malenovský *et al.* 2006; Lukeš *et al.* 2013; Marín *et al.* 2016; Hovi, Raitio and Rautiainen 2017; Abdullah *et al.* 2018) have used an image-capture technique instead to make a more direct and faster determination of the GF. Noda *et al.* (2013) even tried to skip the annoying GF-determination step by attaching a white paper to the back of the sample holder. A recent application of Daughtry's method is to measuring chlorophyll fluorescence spectral properties of needle-shaped leaves (Rajewicz *et al.* 2019).

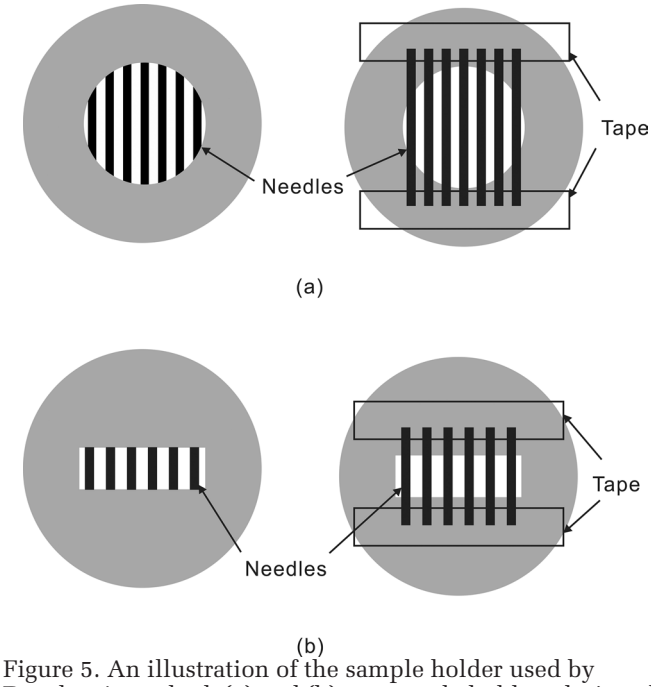

Figure 5. An illustration of the sample holder used by Daughtry's method. (a) and (b) are sample holders designed for long and short conifer needles, respectively. Both the top side (left figures) and underside (right figures) of the sample holders are shown.

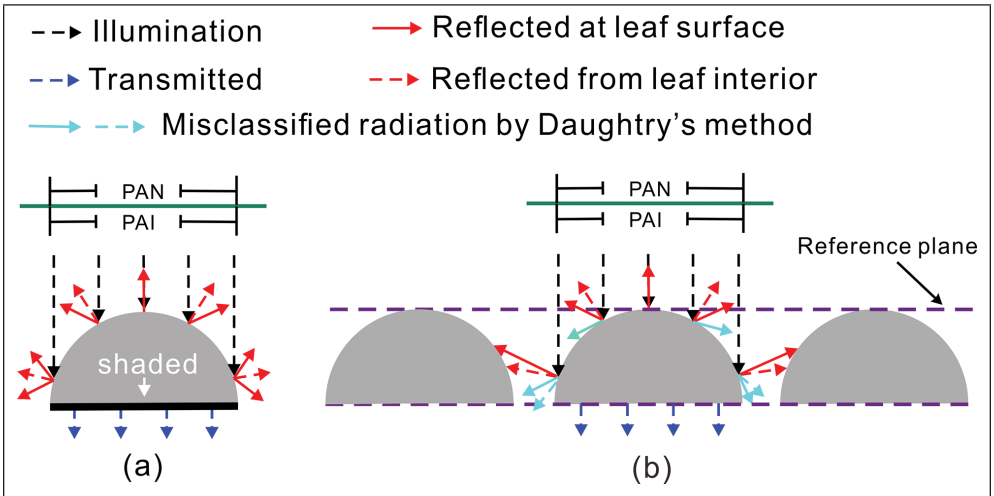

Figure 6. Cross-sectional comparisons between (a) the definition of directional-hemispherical reflectance and transmittance given in the text and (b) Daughtry's method. PAN is the projected area of the needle on a plane perpendicular to the incident direction (green lines). PAI is the projected area of the needle's illuminated surface on a plane perpendicular to the incident direction. All needles are fully illuminated in Daughtry's method, but in this figure, just one needle is illuminated. The reference planes used by Daughtry's method are the two faces of the sample holder (the purple dotted lines). Any radiation penetrating through the upper plane in the opposite direction to incident rays is regarded as reflected radiation; otherwise, it is transmitted radiation, no matter whether it is from the surface or the interior of the needle. The cyan arrows represent the radiation misclassified by Daughtry's method due to the use of an improper reference plane. Multiple scattering of light between needles cannot be avoided in Daughtry's method.

The major drawback of Daughtry's method is that the two faces of the sample holder, rather than the illuminated and shaded surfaces of needles, are the *de facto* reference to distinguish the reflected and transmitted radiation (Figure 6). The radiation scattered at needle edges may penetrate through the sample holder and be counted as transmitted radiation by mistake (Figure 6b). Moreover, multiple scattering between needles is not considered when calculating the final DHR and DHT (shown in Figure 6b). According to Mesarch *et al.* (1999), if interactions between needles are ignored, the optical properties measured by Daughtry's method will be more accurate in samples of smaller GF. However, smaller GF means stronger radiative interactions between needles, which cannot be neglected for accurate spectral measurements. Theoretically, Daughtry's method is able to measure the absorption of needles accurately as long as multiple scattering between needles is neglected, since all reflected and transmitted radiation can be captured—even though they may be misclassified due to the improper reference planes for separating reflected and transmitted radiation (i.e., the faces of sample holder). However, Olascoaga *et al.* (2016) compared the needle absorption measured directly by their revised internal method (needle reflectance and transmittance cannot be measured by this method) with the absorption measured by Daughtry's method under different GFs and found significant differences between these two products. Multiple scattering between needles is likely to be responsible for the inconsistency between the experimental results and our theoretical analysis.

Harron's Method

The reference used by Harron's (2002) method to distinguish reflected and transmitted radiation is one of the faces of the sample holder as well. The main difference between Daughtry's method and Harron's lies in the design of the sample holder. Harron specially molds a pair of black anodized-aluminum carriers with independent slots, each of which holds a needle (Figure 7). In this way, multiple scattering between needles can be eliminated effectively. However, different needle species need different types of carriers, since the slots must fit well to the needles. Moreover, when wrapped in slots, needles cannot be fully exposed to light (as the examples shown in Figure 4), so part of the internally scattered radiation will be absorbed by slot walls, prohibiting a full consideration of the optical properties (Figure 8).

Materials and Methods

Simulating Daughtry's, Harron's, and Defined Reflectance and Transmittance by Ray Tracing

A two-dimensional ray-tracing technique was used to simulate DHR and DHT of needle-shaped leaves. Ray tracing can be implemented by sending massive rays and tracing the reflection, transmission, scattering, and absorption of each ray at leaf surfaces or within the leaf interior. Summing over the reflected and transmitted fluxes of all rays and dividing by the total incident flux produces the final reflectance and transmittance.

There are three sets of DHR and DHT to compare in this study: those simulated based on Daughtry's and Harron's protocols and the definitions given in the present study. Hereafter, they are called Daughtry's, Harron's, and reference and transmittance. With the help of ray tracing, differences among these three sets of reflectance and transmittance were investigated for two needle shapes (triangular and semicircular) when collimated light was incident on different needle sides (flat or convex; Table 1). In order to simplify the radiative transfer of rays, the leaf interior was assumed to be homogeneous. Possible mutual masking created by leaf roughness (Bousquet *et al.* 2005), the hot spot (Comar *et al.* 2012), and scattering happening inside needles were neglected. All the needles were supposed to have rough surfaces, which was implemented in codes by giving needle surfaces a random tilt angle to ensure an incident angle in [0°, 40°] for rays traveling from air to needle (Bousquet *et al.* 2005) and one in [0°, 90°] for rays traveling from needle to air. The refraction and

Figure 7. A photo of the sample holder used in Harron's method (Zhang *et al.* 2008).

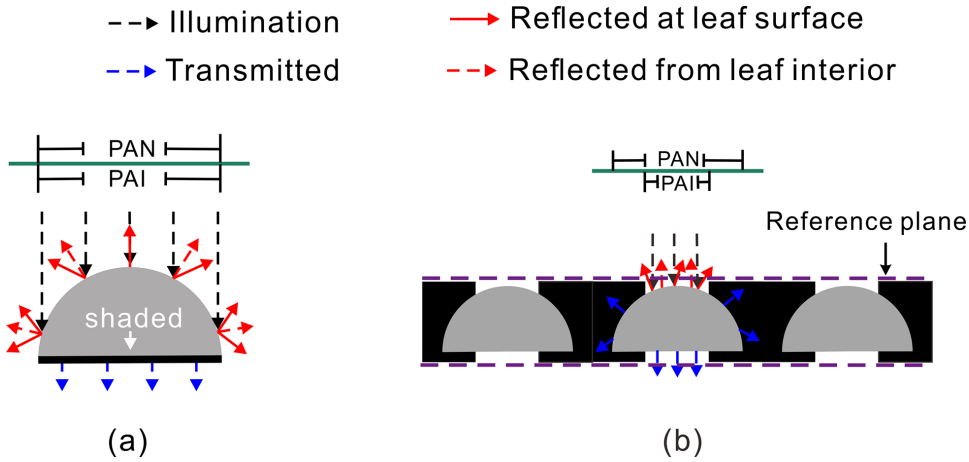

Figure 8. Cross-sectional comparisons between (a) the definition of directional-hemispherical reflectance and transmittance given in the text and (b) Harron's method. PAN is the projected area of the needle on a plane perpendicular to the incident direction (green lines). PAI is the projected area of the needle's illuminated surface on a plane perpendicular to the incident direction. All needles are partially illuminated in Harron's method, but in this figure, just one needle is illuminated. The reference planes used by Harron's method are the two faces of the sample holder (the purple dotted lines). All the radiation penetrating through the upper plane in the opposite direction to incident rays is regarded as reflected radiation; otherwise, it is transmitted radiation. Multiple scattering of light between needles can be eliminated effectively in Harron's method, but some radiation will be absorbed by the sample holder, prohibiting a full consideration of the optical properties.

reflection happening at needle surfaces were quantified by Fresnel equations and Snell's law, while the absorption by leaf tissues was calculated by the Beer–Lambert law. Four biochemical constituents were included. They are chlorophyll, carotenoid, water, and dry matter. Absorption coefficients of these four constituents as well as leaf surface refractive indices were taken from PROSPECT-5 (Feret *et al.* 2008).

The needles used in ray tracing are simplexes, not microscopic anatomical images of real needles, for three reasons: The anatomical structures of real leaves are too complex; it requires too much computation to trace the optical properties of needles by microscopic images, because multiple complicated processes are involved, such as vectorization; and no matter what the object being measured is, the differences between Daughtry's method, Harron's method, and our definition can always be investigated as long as the object is same for all methods. We have maintained primary physical and chemical traits of real needles (leaf surface roughness, needle shape, and biochemical constituents) as much as we can, but even so, the ray-tracing technique is not guaranteed to produce real and accurate needle reflectance and transmittance.

The ray number and tracing repetitions need to be optimized to avoid excessive tracing as well as to save computational costs. Less noise was observed with more rays (Figure 9a), but the spectra basically overlapped after being smoothed with a 10-nm moving-window averaging scheme (Figure 9b). Thus, 1500 rays were sent in this study. The radiant flux of a ray decreased when the ray was traced more times, and can be neglected after 10 tracings (Figure 9c). Therefore, the tracing repetitions were set to be 10 for all rays.

In this study, the reference reflectance and transmittance were treated as the benchmark based on which the absolute error (AE) and relative error (RE) of Daughtry's and Harron's reflectance, transmittance, and absorption were calculated, according to the equations

$$\mathrm{AE}(\lambda) = S^*(\lambda) - S(\lambda) \tag{1}$$

$$\mathrm{RE}(\lambda) = [S^*(\lambda) - S(\lambda)]/S(\lambda), \tag{2}$$

where $S^*(\lambda)$ represents Daughtry's or Harron's reflectance, transmittance, or absorption at wavelength λ and $S(\lambda)$ denotes the corresponding reference reflectance, transmittance, or absorption.

Demonstrating the Incompleteness of Harron's Reflectance and Transmittance Indirectly by Model Inversions

One of the main conclusions drawn in this study is that DHR and DHT measured by Harron's method can be incomplete, which will result in prominent overestimation of needle absorption. This conclusion can be proved by inversions of an optical-properties model. Existing optical-properties models are built on the same basic premise: the sum of reflectance R, transmittance T, and absorption A equals 1—that is,

$$R+T+A=1. \tag{3}$$

If leaf absorption is overestimated, it will result in overestimation of leaf biochemical contents. So if significant positive biases are observed for estimated biochemical constituents, the absorption is overestimated, in support of our conclusion.

In this study, the PROSPECT-5 model (Jacquemoud and Baret 1990; Féret *et al.* 2008) was chosen. There are other optical-properties models, such as LIBERTY (Dawson, Curran and Plummer 1998), LEAFMOD (Ganapol *et al.* 1998), and SLOP (Maier, Lüdeker and Günther 1999). We chose PROSPECT-5 because it has been widely used in the remote-sensing community. The LIBERTY model, which was developed for needle-shaped leaves, was not used in this study because several potential flaws in its physical architecture have been found (Wang and Ju 2017).

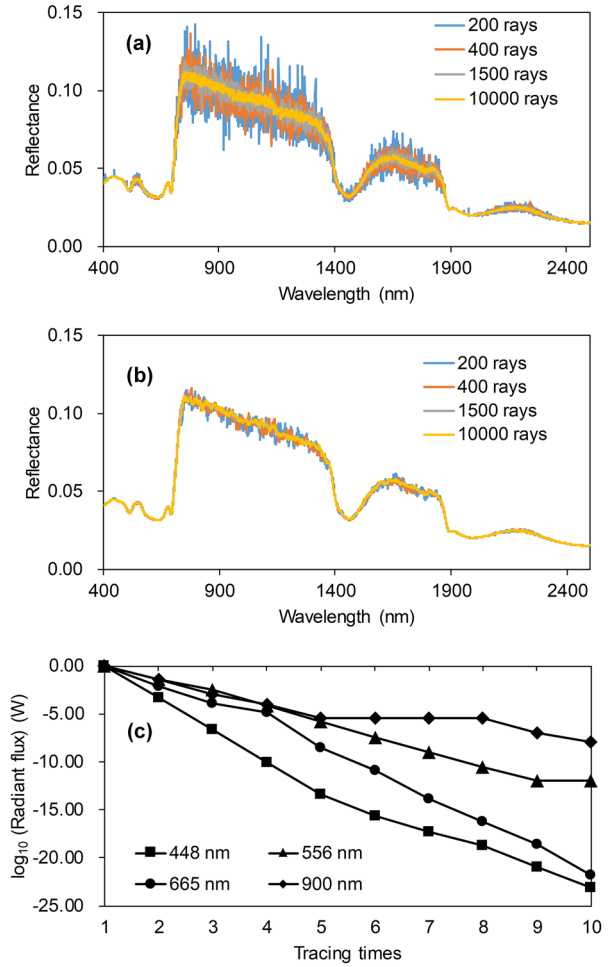

Figure 9. Determination of ray number and tracing repetitions. (a) Simulated needle reflectance spectra when different numbers of rays are deployed. The needle has a semicircular cross section and light is incident on the convex side of the needle. The concentrations of chlorophyll, total carotenoid, water, and dry matter are set to be, respectively, 720 µg/cm³, 160 µg/cm³, 0.34 g/cm³, and 0.07 g/cm³. (b) The reflectance spectra smoothed with a 10-nm moving-window averaging scheme. (c) Change in the radiant flux of a ray (log transformed) with tracing repetitions inside the needle. The initial value of the radiant flux is assumed to be 1 W.

We did not recalibrate parameters of PROSPECT-5 for needles as Malenovský *et al.* (2006) did, because such calibrations are not necessary if the measured spectra are likely to be inaccurate, which we have already theoretically explained.

Model inversion, in essence, is to find the optimal combination of the input parameters to minimize the difference between simulated and measured optical spectra. This can be achieved by minimizing the merit function

$$K(N, C_1, \ldots, C_n) = \sum_{\lambda} [(R_{\mathrm{mod}}(\lambda) - R_{\mathrm{mes}}(\lambda))^2 + (T_{\mathrm{mod}}(\lambda) - T_{\mathrm{mes}}(\lambda))^2 \tag{4}$$

where N is the structural parameter in PROSPECT-5; $C_1, \ldots, C_n$ are biochemical constituents to be estimated; $R_{\mathrm{mes}}(\lambda)$ and $T_{\mathrm{mes}}(\lambda)$ are the measured reflectance and transmittance at the wavelength λ (nm); and $R_{\mathrm{mod}}(\lambda)$ and $T_{\mathrm{mod}}(\lambda)$ are the modeled reflectance and transmittance. The optimization is performed using a constrained Powell line search for finding the minimum of the merit function. The parameterization of the method can be found in Table 3.

Since only chlorophyll and carotenoid are available in this study, to explore the influences of the measured partial reflectance and transmittance on model inversions we first run the PROSPECT-5 model in backward mode, with the spectral range restricted to 400–690 nm and the absorption assumed to be determined only by chlorophyll and carotenoid (Scheme 1). The spectral range was selected according to the absorption coefficient spectra available in this model. To allay concerns about the influences of other biochemical constituents on the inversion results, another scheme (Scheme 2) was also carried out. In this scheme, PROSPECT-5 was run in backward mode to estimate chlorophyll, carotenoid, equivalent water thickness, and leaf mass per area simultaneously using the spectral information of 400–900 nm. Wavelengths longer than 900 nm were removed due to low signal-to-noise ratio. Finally, the coefficient of determination (R^2) and relative mean standard error (RMSE) were calculated for both chlorophyll and carotenoid.

Data

Study Sites and Needle Sampling

Four field experiments were carried out in June, July, and August of 2003 and August of 2004 near Sudbury, Ontario, Canada (46°49′13″ N to 47°12′9″ N, 81°22′2″ N to 81°54′30″ N), where 10 large black spruce (*Picea mariana* (Mill.)) stands were selected as study sites. In each site, five trees were marked for sampling. Usually, one shoot is taken from each tree for subsequent spectral measurements and chemical analysis. But some trees had obvious young or old needles, and therefore additional shoots were sampled for these trees. In August of 2004, a medium-sized tree from one mature site was selected to analyze the influences of needle age and branch orientation on the variation of needle optical, biophysical, and biochemical parameters. Four shoots were sampled from this tree from four orientations—i.e., north, south, east, and west branches. Needles of different age classes (1998–2004) were taken from each shoot for biochemical measurements. There were 91 samples in total, but four were discarded due to loss of the spectra file. In the end, only 87 samples were available in this study.

Measurements of Needle Optical Properties

Harron's method was adopted to measure the reflectance and transmittance of black-spruce needles. The equipment used in this method include a FieldSpec Pro FR spectroradiometer (Analytical Spectral Devices, Inc., Boulder, Colo.) and a LI-COR 1800-12S integrating sphere (LI-COR, Inc., Lincoln, Neb.). They were connected with each other via an optical fiber. The spectroradiometer captures signals from the integrating sphere and produces spectra ranging from 350 to 2500 nm at 1-nm intervals. There are five ports in the integrating sphere. The measurements include the reference signal (RSS), the transmittance signal (TSP), the reflectance internal standard (RTS), the reflectance ambient (RSA), and the dark measurement (DRK). The detailed configurations of the integrating sphere for these five parameters are listed in Table 2 and illustrated in Figure 10. The DHR and DHT of leaves were calculated as

$$\mathrm{DHR}(\lambda) = \left(\frac{\mathrm{RSS}-\mathrm{RSA}}{\mathrm{RTS}-\mathrm{RSA}}\right)\cdot R_r(\lambda) \quad (5)$$

$$\mathrm{DHT}(\lambda) = \left(\frac{\mathrm{TSP}-\mathrm{DRK}}{\mathrm{RTS}-\mathrm{RSA}}\right)\cdot R_r(\lambda) \quad (6)$$

Table 2. Configuration of the integrating sphere in Figure 10.

Parameter	Port A	Port B	Port C	Port D	Port E
RSA	L	W	EC	P	P
RSS	L	W	C	P	P
RTS	L	C	W	P	P
TSP	P	W	O	L + C	P
DRK	P	W	C	L (power off)	P

C = sample holder with samples; DRK = dark measurement; EC = empty sample holder; L = light source; O = empty port with light trap; P = white plug; RSA = reflectance ambient; RSS = reference signal; RTS = reflectance internal standard; TSP = transmittance signal; W, white reference.

Table 3. Maximum, minimum, and initial values for PROSPECT-5 in the backward inversion.

Statistic	N	C_{ab} (µg/cm²)	C_{xc} (µg/cm²)	EWT (cm)	LMA (g/cm²)
Maximum	6	150	30.0	0.100	0.0300
Minimum	1	8	0.0	0.001	0.0010
Initial	3	28	6.3	0.011	0.0054

C_{ab} = chlorophyll a + b; C_{xc} = total carotenoid; EWT = equivalent water thickness; LMA = leaf mass per area; N = number of plates (the structural parameter in PROSPECT-5).

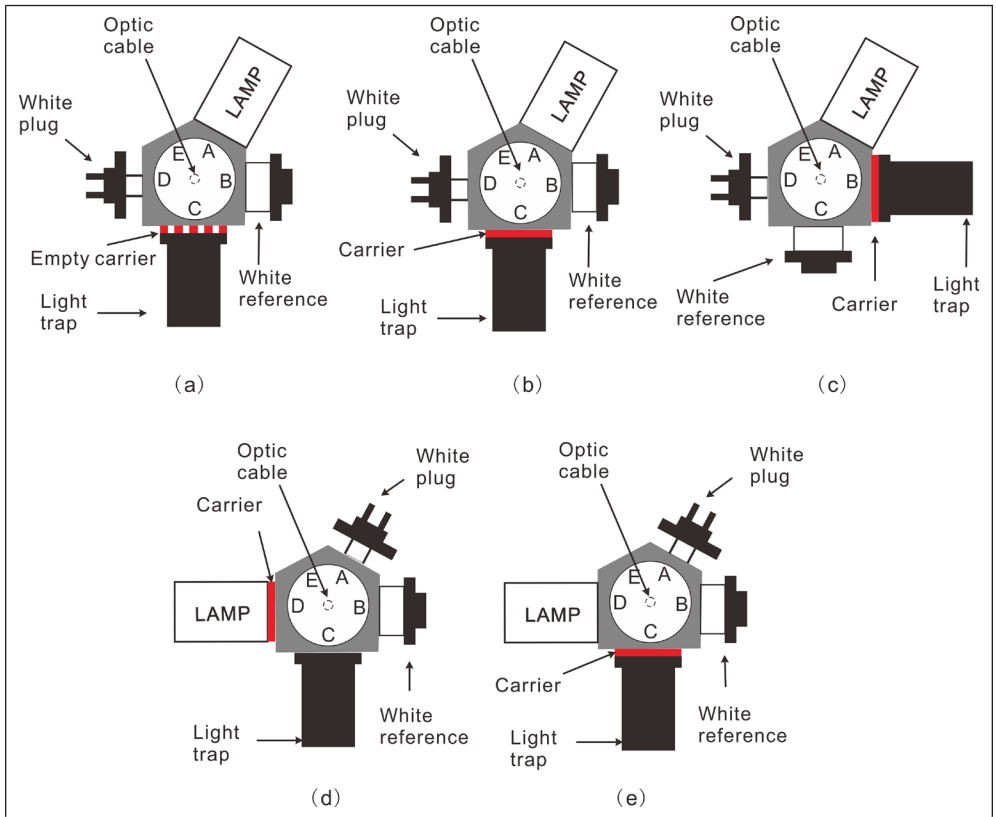

Figure 10. Examples of integration-sphere configurations. (a) reflectance ambient (RSA) in Table 2; (b) reference signal (RSS) in Table 2; (c) reflectance internal standard (RTS) in Table 2; (d) transmittance signal (TSP) in Table 2; (e) dark measurement (DRK) in Table 2; Port E has a white plug in all configurations.

where $R_r(\lambda)$ is the reflectance of the calibrated reference standard at wavelength λ (nm), which has been provided by the manufacturer of the integrating sphere. Other parameters needed in Equations 5 and 6 are listed in Table 2.

A pair of black anodized-aluminum carriers designed by Harron (2002) were used in this study to hold needle samples. Five needles were mounted in the five independent slots of the carriers against the sample port of the integrating sphere during measurements. Harron's protocol has been evaluated in detail with Boreal Ecosystem-Atmosphere Study (BOREAS; RSS-04 1994) data on the jack pine.

Measurements of Needle Biophysical Properties and Chlorophyll Contents

Following the needle optical measurements, the width and thickness of individual needles were measured using a digital caliper (Marathon Company, City, Canada). The needles were then stored in separate freezer bags and placed in a cooler with ice (0°C) for transport to a laboratory and stored at −23°C after arrival. Further measurements were conducted in a laboratory of the Ontario Forest Research Institute before the needles were dehydrated and shrunk. Needle chlorophyll content was measured using the method described by Moorthy, Miller, and Noland (2008). Table 4 provides a summary of the measured structural parameters, chlorophyll content (C_{ab}), and total carotenoid content (C_{xc}). Descriptions of the black-spruce data set are also given by Zarco-Tejada *et al.* (2004) and Zhang *et al.* (2008).

Table 4. Statistics of the structural parameters, chlorophyll content (C_{ab}), and total carotenoid content (C_{xc}) of the black-spruce data set.

Statistic	Width (cm)	Thickness (cm)	C_{ab} (µg/cm^2)	C_{xc} (µg/cm^2)
Minimum	0.11	0.07	11.97	3.18
Maximum	0.22	0.12	48.71	10.29
Mean ± SD	0.16 ± 0.03	0.09 ± 0.01	28.95 ± 8.62	6.33 ± 1.62

Results

Accuracy of Daughtry's and Harron's Methods

We compared Daughtry's and Harron's reflectance and transmittance with the reference reflectance and transmittance of the same needle shape simulated under the same illumination conditions (Figure 11) and found that both Daughtry's and Harron's reflectance and transmittance are biased with respect to the reference. Moreover, the bias varies with wavelength.

There are larger discrepancies for Daughtry's method when measuring reflectance and transmittance at wavelengths in the near-infrared region (NIR, 800–1400 nm) and shortwave infrared (1500–1900 nm), where light is rarely absorbed. However, at wavelengths with strong absorption characteristics, such as the visible spectral region and the atmospheric window, this method shows better performance. A trade-off was found between the biases of Daughtry's reflectance and transmittance (Figure 12b). Therefore, the absorption measured by Daughtry's method agrees well with the reference absorption across the whole spectral range (400–2500 nm) if and only if multiple scattering between needles is neglected.

By contrast, Harron's reflectance and transmittance contain larger errors than Daughtry's. Both the reflectance and transmittance were underestimated across the whole spectral range compared with the reference, with more obvious underestimation in weak-absorbing spectral regions, resulting in significant overestimation of the needle absorption.

Influence of Incident Direction of Light on the Accuracy of Daughtry's and Harron's Methods

Daughtry's reflectance and transmittance were biased regardless of the incident direction (max|RE|>50%), while no obvious bias was observed for the absorption (Figure 12), due to the trade-off between the biases of the reflectance and transmittance. So Daughtry's method will not underestimate or overestimate needle absorption if multiple scattering between needles is not considered.

When light struck on the flat sides of the needles, Daughtry's reflectance was overestimated and transmittance underestimated, whereas when it struck on the convex sides, the reflectance and transmittance were underestimated and overestimated, respectively, demonstrating the great influence of incident direction on accuracy with Daughtry's method.

The error of Daughtry's reflectance changed little across the whole spectral region when the convex sides of the needles were illuminated. But the transmittance showed much larger biases in strongly absorbing some spectral regions than others (|RE| ≈ 40% near 400 nm). When the flat sides of the needles were illuminated, the reflectance contained greater errors at wavelengths where light is weakly absorbed (|RE|>50%) than at other wavelengths, but the relative error of transmittance was smaller than 10%.

Both Harron's reflectance and transmittance were negatively biased, while absorption was positively biased no matter whether the convex or flat sides of the needles were illuminated. The most

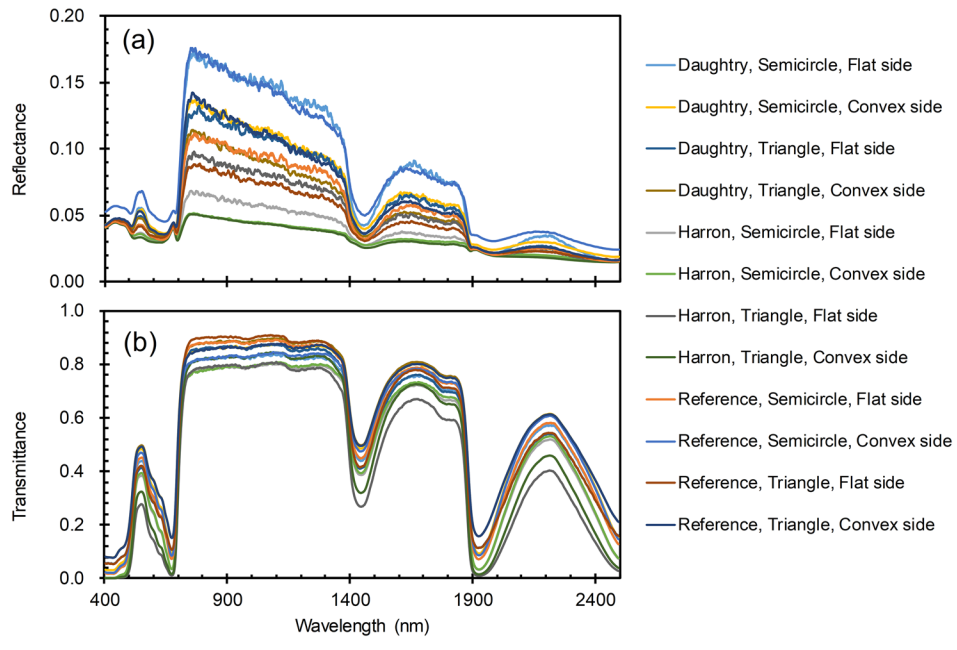

Figure 11. Simulated directional-hemispherical (a) reflectance and (b) transmittance spectra of needles with different shapes under different measurement protocols. Measurement technique, needle shape, and incident direction are noted in the legend. The concentrations of chlorophyll, total carotenoid, water, and dry matter are set to be, respectively, 720 µg/cm^3, 160 µg/cm^3, 0.34 g/cm^3, and 0.07 g/cm^3. The needle width is 0.15 cm. The slot width of Harron's method is set to 0.075 cm. The refractive indices are taken from PROSPECT-5.

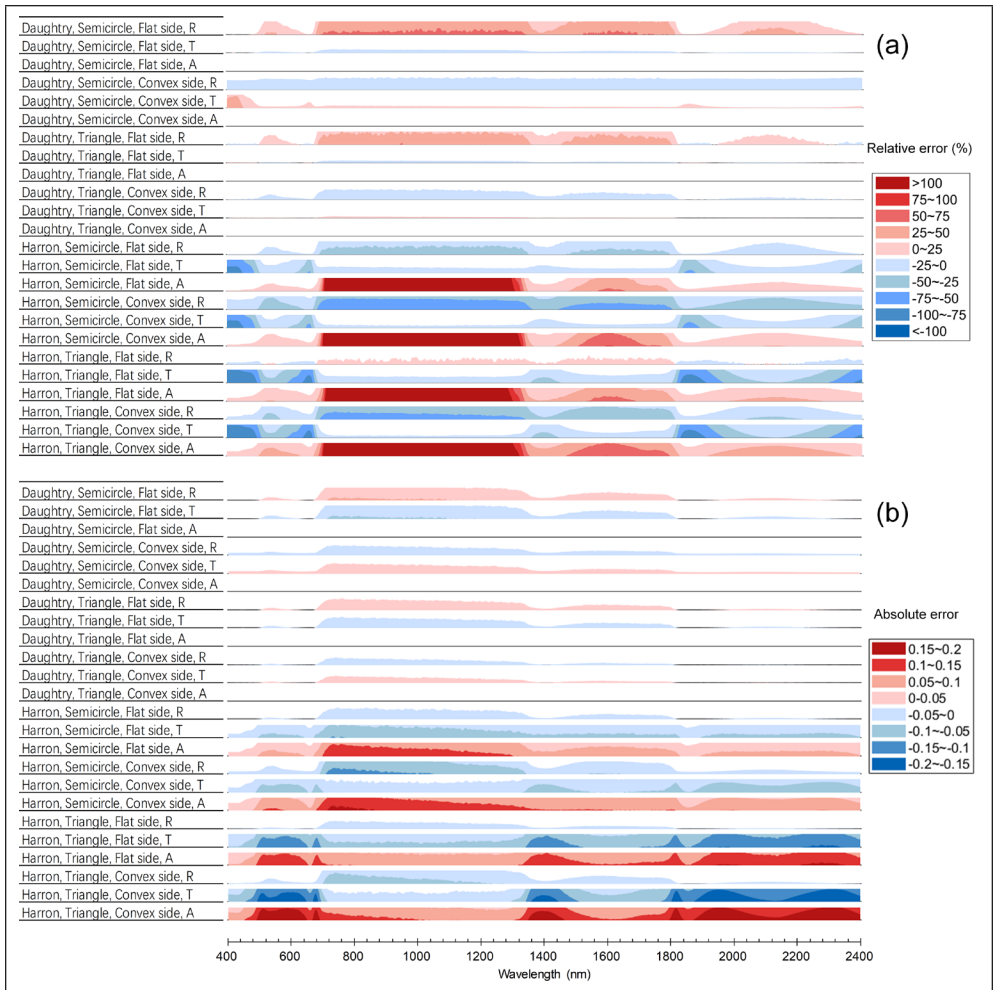

Figure 12. Horizon graph of (a) relative error and (b) absolute error of all simulated spectra. Measurement technique, leaf shape, incident direction, and spectrum type are given in the left panel. The color represents the range of error, while the height of the area plot indicates the difference between the positive relative or absolute error and the lower bound of the corresponding range (for negative relative or absolute error, the upper bound of the range). The concentrations of chlorophyll, total carotenoid, water, and dry matter are set to be, respectively, 720 μg/cm^3, 160 μg/cm^3, 0.34 g/cm^3, and 0.07 g/cm^3. The needle width is 0.15 cm. Relative errors of Daughtry's absorption lie in the range of –25% to 25%. The refractive indices are taken from PROSPECT-5. The error is assessed with respect to the reference proposed in this study (Equations 1 and 2).

shocking overestimation of absorption happened in NIR ($|RE| \approx 1500\%$; see Figure 12).

In general, the reflectance was measured more accurately when light was incident on the flat sides of the needles, for both Daughtry's and Harron's methods.

Influence of Needle Shape and Size on the Accuracy of Daughtry's and Harron's Methods

The errors of both methods varied with needle shape (Figure 11 and 12). NIR and shortwave infrared were the spectral regions where the largest errors of reflectance appeared. Without considering multiple scattering between needles, the absorption of needles could be measured accurately by Daughtry's method regardless of needle shape. In contrast, the absorption simulated with Harron's method was obviously overestimated, and its accuracy was more sensitive to needle shape.

Significant but wavelength-dependent differences were observed between the reflectance and transmittance of needles of different sizes regardless of measurement method (Figure 12). Increasing needle size exhibited a rising trend in needle transmittance, particularly evident in strongly absorbing spectral regions such as the visible spectral region (Figure 13). In terms of accuracy, the relative and absolute errors of Daughtry's and Harron's reflectance and transmittance changed little with needle size (Figures 14 and 15), indicating marginal influence of needle size on the precision of Daughtry's method. The absolute errors of Harron's reflectance, transmittance, and absorption were stable across different needle sizes, but the relative error of absorption changed dramatically due to the critical variations in the reference absorption (Equation 2).

Influence of Leaf Biochemical Parameters on the Accuracy of Daughtry's and Harron's Methods

Both Daughtry's and Harron's transmittance in the visible domain shrank (Figure 16), with decreasing absolute error (Figure 17), as chlorophyll concentration increased. The largest error appeared at green wavelengths near 555 nm, where relatively less radiation was absorbed by the needles.

Daughtry's method showed excellent performance in the blue spectral domain (400–500 nm in Figure 6). When light struck the flat sides of the needles, the absolute errors of Daughtry's reflectance and transmittance in this domain were close to 0; by contrast, those of Harron's transmittance were much larger.

No bias was found for Daughtry's absorption, no matter what the chlorophyll concentration of the needle. Harron's absorption was significantly overestimated compared with the reference.

Influence of the Sample Holder's Aperture Width on the Accuracy of Harron's Method

Figure 19 displays the variations of Harron's reflectance and transmittance with the aperture width of the sample holder under the same needle shape and incident direction. The wider the aperture, the more accurate Harron's method was. When the aperture width is equal to the needle width or larger, Harron's method actually measures the defined benchmark reflectance and transmittance. The absorption of needles will always be underestimated by Harron's method as long as the aperture width is smaller than the needle width.

Influence of Mutual Shadowing Between Needles on the Accuracy of Daughtry's Method

Through comparing Daughtry's reflectance and transmittance of needle mats (three needles side by side) and individual needles, surprising needle-shape-independent consistencies arose between these two spectra sets across the whole spectral range (Figure 20), suggesting a marginal influence of mutual shadowing between needles on the accuracy of Daughtry's method.

PROSPECT-5 Inversions

When just chlorophyll and carotenoid contents were estimated with the PROSPECT-5 model, pronounced overestimation was observed for both pigments (Scheme 1 in Figure

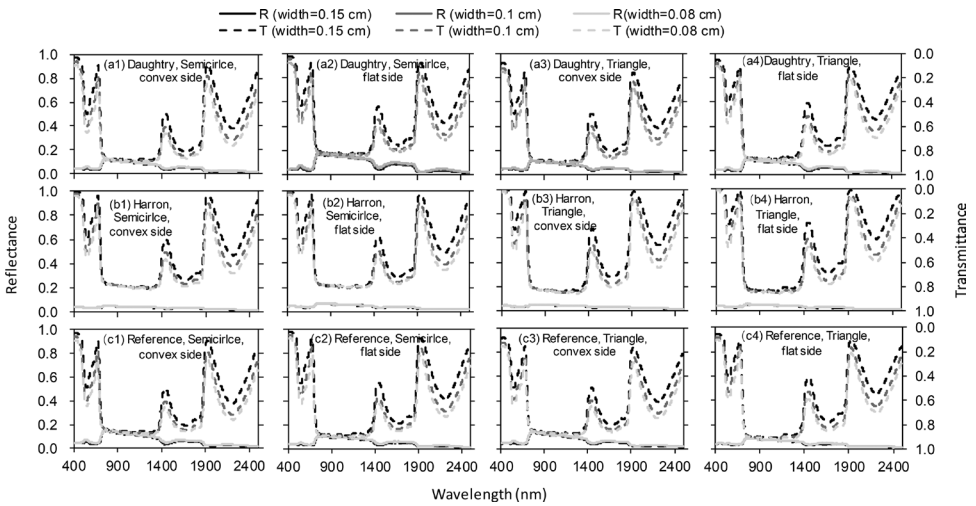

Figure 13. Daughtry's, Harron's, and defined reflectance and transmittance of different-size needles. The captions convey information about measurement protocol, needle shape, and incident direction of light. The concentrations of chlorophyll, total carotenoid, water, and dry matter are set to be, respectively, 720 µg/cm^3, 160 µg/cm^3, 0.34 g/cm^3, and 0.07 g/cm^3. The refractive indices are taken from PROSPECT-5. The slot width for Harron's method is set to half the needle width.

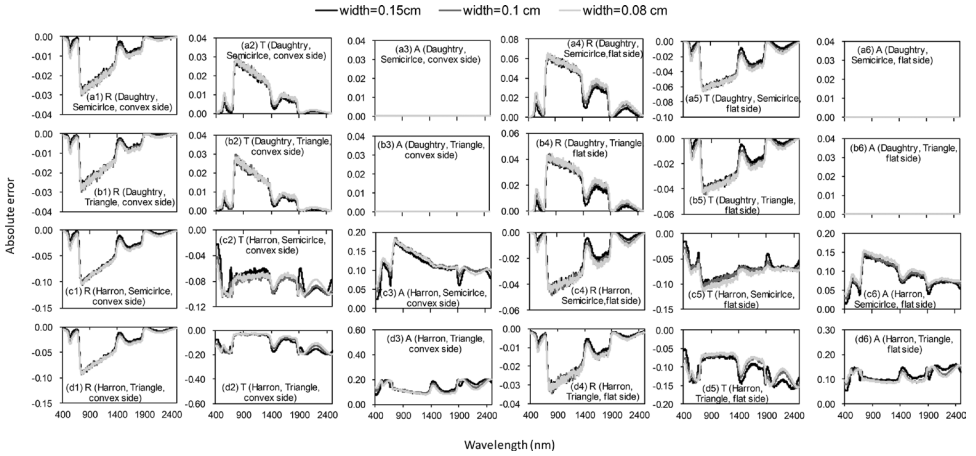

Figure 14. Absolute error of Daughtry's and Harron's methods for different-size needles. The captions convey information about spectral type, measurement technique, needle shape, and incident direction of light. The concentrations of chlorophyll, total carotenoid, water, and dry matter are set to be, respectively, 720 µg/cm^3, 160 µg/cm^3, 0.34 g/cm^3, and 0.07 g/cm^3. The refractive indices are taken from PROSPECT-5. The slot width for Harron's method is set to half the needle width. The error is assessed with respect to the reference proposed in this study (Equations 1 and 2).

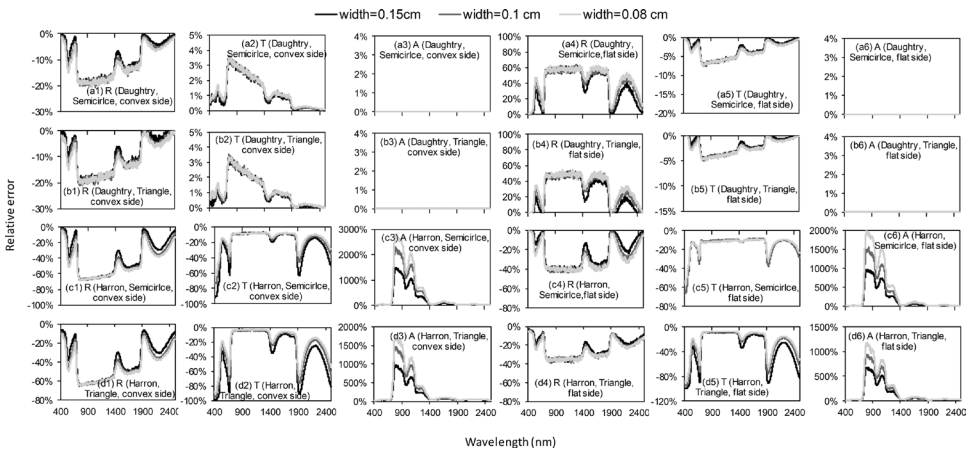

Figure 15. Relative error of Daughtry's and Harron's methods for different-size needles. The captions convey information about spectral type, measurement technique, needle shape, and incident direction of light. The concentrations of chlorophyll, total carotenoid, water, and dry matter are set to be, respectively, 720 µg/cm^3, 160 µg/cm^3, 0.34 g/cm^3, and 0.07 g/cm^3. The refractive indices are taken from PROSPECT-5. The slot width for Harron's method is set to half the needle width. The error is assessed with respect to the reference proposed in this study (Equations 1 and 2).

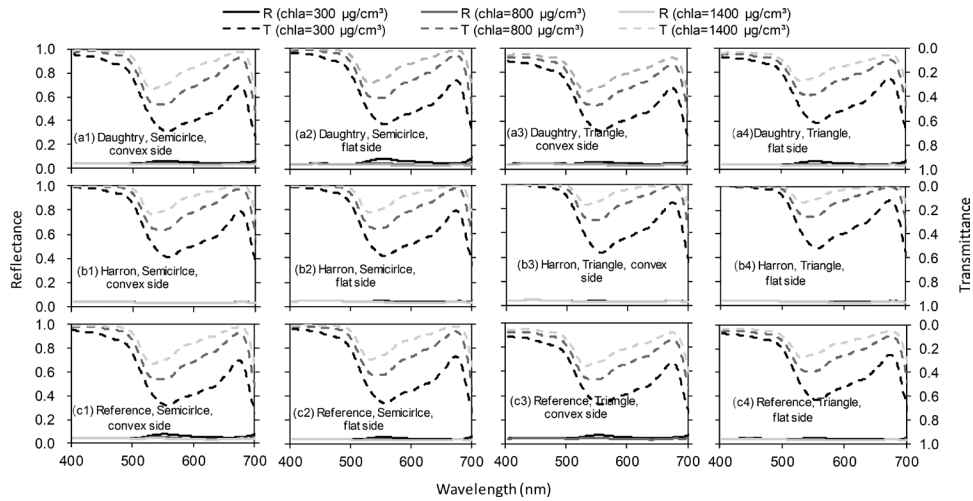

Figure 16. Daughtry's, Harron's, and defined reflectance and transmittance (visible spectral region: 400–700 nm) of needles with different chlorophyll concentrations. The captions convey information about measurement protocol, needle shape, and incident direction of light. The concentrations of total carotenoid, water, and dry matter are set to be, respectively, 160 µg/cm^3, 0.34 g/cm^3, and 0.07 g/cm^3. The refractive indices are taken from PROSPECT-5. The needle width is 0.15 cm. The slot width for Harron's method is set to 0.075 cm.

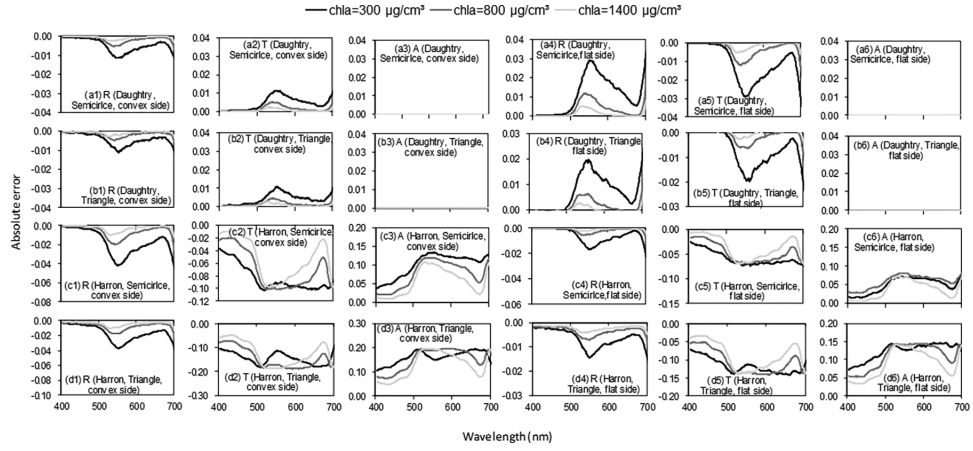

Figure 17. Absolute error of Daughtry's and Harron's methods for needles with different chlorophyll (chla) concentrations. The captions convey information about measurement technique, needle shape, and incident direction of light. The concentrations of total carotenoid, water, and dry matter are set to be, respectively, 160 µg/cm^3, 0.34 g/cm^3, and 0.07 g/cm^3. The refractive indices are taken from PROSPECT-5. The error is assessed with respect to the reference proposed in this study (Equations 1 and 2).

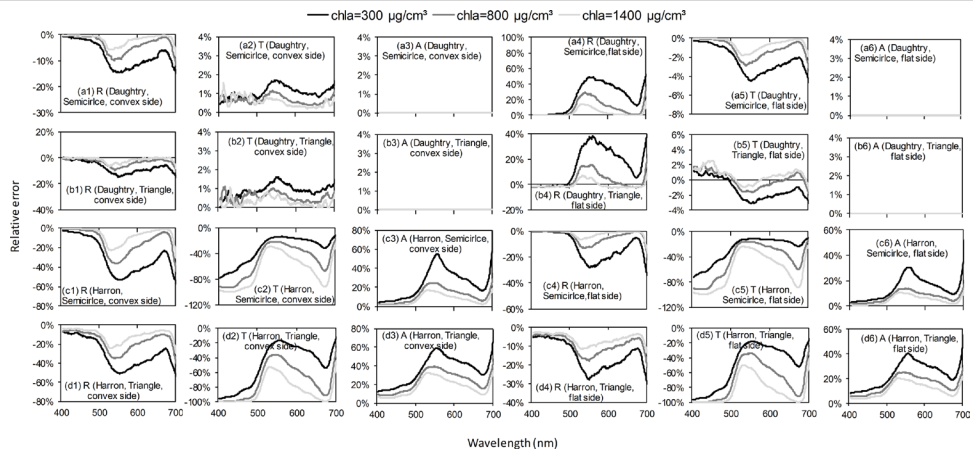

Figure 18. Relative error of Daughtry's and Harron's methods for needles with different chlorophyll (chla) concentrations. The captions convey information about spectral type, measurement technique, needle shape, and incident direction of light. The concentrations of total carotenoid, water, and dry matter are set to be, respectively, 160 µg/cm^3, 0.34 g/cm^3, and 0.07 g/cm^3. The refractive indices are taken from PROSPECT-5. The error is assessed with respect to the reference proposed in this study (Equations 1 and 2).

21a and 21b). The overestimation of chlorophyll was not alleviated when more kinds of biochemical constituents were added into the model inversion (Scheme 2 in Figure 21a), demonstrating that the overestimation is not caused by the inversion strategy. The model failed to estimate the carotenoid content of black-spruce needles (R^2 = 0.087) when other biochemical constituents, such as equivalent water thickness and leaf mass per area, were added. These observations are similar to the finding by Féret *et al.* (2019) that PROSPECT shows better performance in the estimation of leaf mass per area and equivalent water thickness when using spectral information from 1700 to 2400 nm than when using broader spectral ranges.

There are two causes that might be responsible for the failure of carotenoid estimation in Scheme 2. First, Harron's method is compromised and will cause overestimation of absorption, which cannot be quantified and may vary across samples. Second, the absorption of carotenoid is shaded by that of chlorophyll. The absorption of carotenoid is prominent in 400–560 nm. Above 560 nm, chlorophyll dominates the absorption. Dry matter also shows significant absorption in 400–560 nm. The mechanism of PROSPECT-5 inversion is to sum all the squared errors between measured and estimated reflectance and transmittance across the whole spectral range of interest and find the minimum of the least-square-based sum (Equation 4). So if the selected spectral range is wider than the absorption features of carotenoid and chlorophyll, and other constituents such as water and dry matter are added, the accuracy of carotenoid and chlorophyll estimations will degrade. The results prove that the measured biased reflectance and transmittance will cause an overestimation of the biochemical contents of needle-shaped leaves.

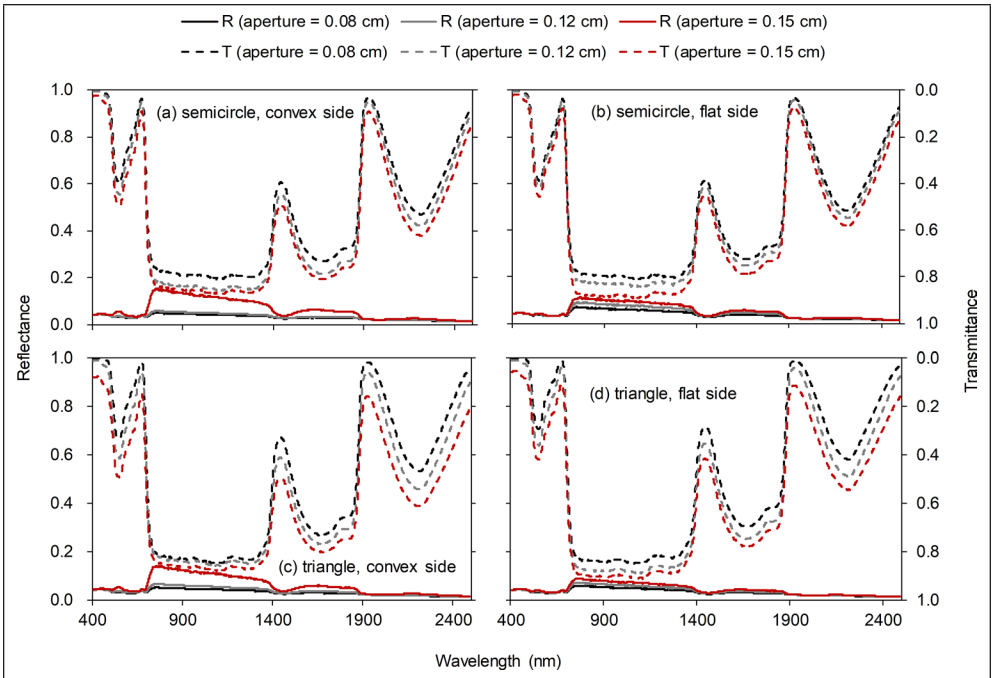

Figure 19. Harron's reflectance and transmittance when carriers with different slot widths are used. The captions convey information about needle shape and incident direction. The concentrations of total carotenoid, water, and dry matter are set to be, respectively, 160 µg/cm³, 0.34 g/cm³, and 0.07 g/cm³. The refractive indices are taken from PROSPECT-5. The needle width is 0.15 cm.

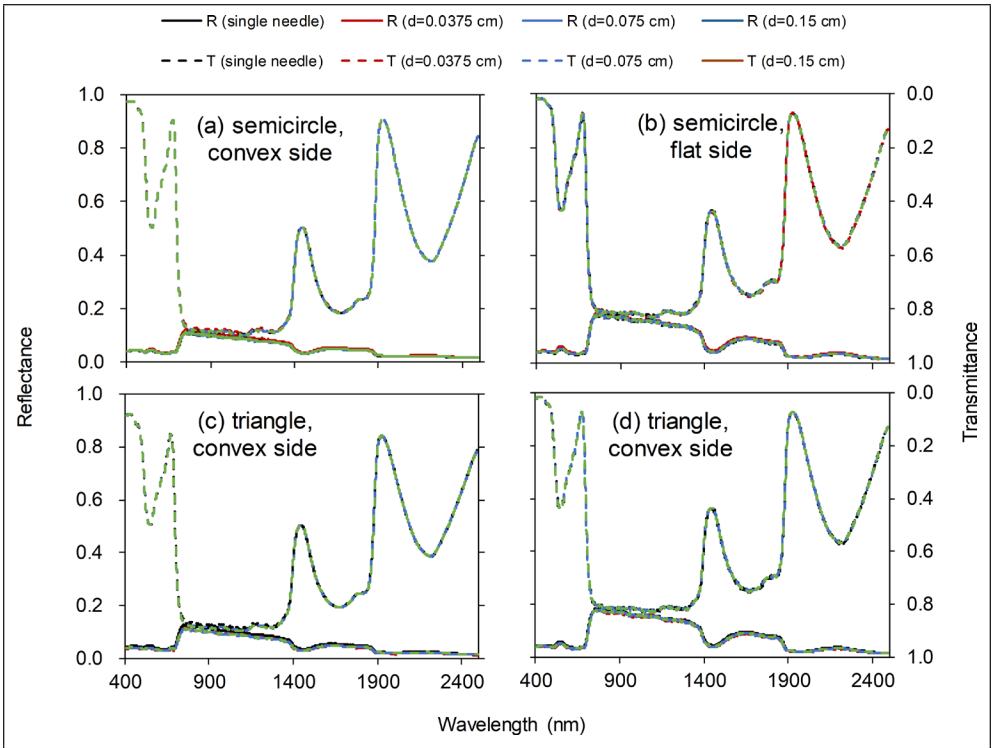

Figure 20. Daughtry's reflectance and transmittance of three needles arranged with different gap sizes. The concentrations of chlorophyll, total carotenoid, water, and dry matter are set to be, respectively, 720 µg/cm³, 160 µg/cm³, 0.34 g/cm³, and 0.07 g/cm³. The refractive indices are taken from PROSPECT-5.

Discussion

Leaf DHR and DHT play an important role in both leaf-scale and canopy-scale remote-sensing studies. At the leaf scale, they are the fundamental data for leaf biochemical constituent inversions, using either spectral-index models or leaf optical-properties models. At the canopy scale, leaf DHR and DHT are often needed to evaluate or eliminate the influences of canopy structure and background on canopy reflectance (e.g., Zhang *et al.* 2008; Croft *et al.* 2015). If collected leaf spectra are compromised, remote-sensing models developed based on them will also be compromised, leading to problematic applications to biochemical parameter retrieval.

Due to needles' narrow and thick morphological characteristics, a clear understanding of how to distinguish between reflected and transmitted radiation is needed for the sake

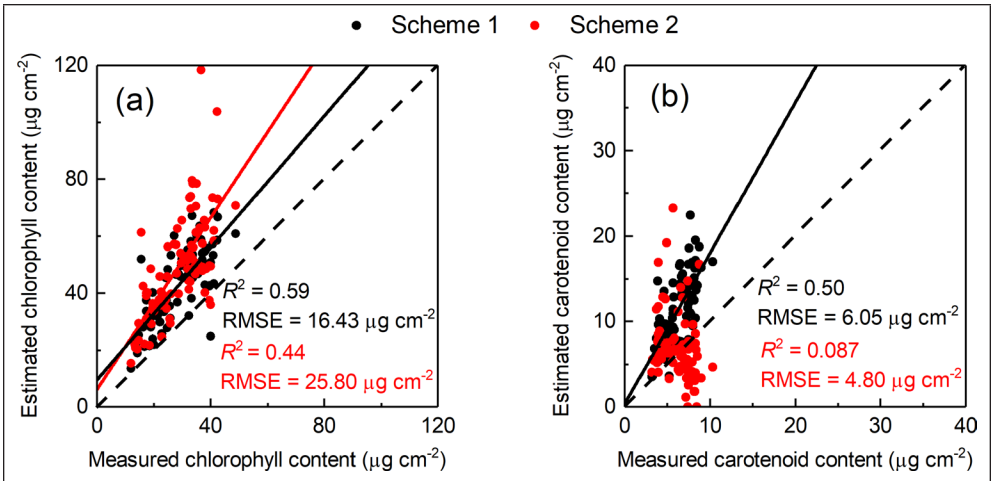

Figure 21. Results of PROSPECT-5 inversions of (a) chlorophyll and (b) total carotenoid over the black-spruce data set. The coefficients of determination (R^2) and relative mean squared error (RMSE) were calculated. Scheme 1 (black points) is to estimate only chlorophyll and carotenoid using wavelengths of 400–690 nm. Scheme 2 (red points) is to estimate chlorophyll, carotenoid, equivalent water thickness (EWT), and leaf mass per area (LMA) simultaneously using wavelengths of 400–900 nm.

of accurate reflectance and transmittance measurement; but unfortunately, this issue has not been addressed with existing techniques. This study investigated primary integrating-sphere-based spectral measurement methods for needle-shaped leaves from a theoretical point of view and gives a definition that may be helpful for the development of new measurement techniques.

Daughtry's method measures the reflectance and transmittance of needles with opposite biases, resulting in high accuracy in needle absorption measurement. The biases in reflectance and transmittance are more prominent in spectral regions characterized by weak absorption, such as NIR, than in other spectral regions. When an incident ray strikes on the surface of a needle, most (>90%) of the energy of this ray will penetrate through the surface and interact with the leaf interior according to Fresnel equations, but little radiation arrives at the shadow surface after perhaps one pass from the illuminated surface if the ray is strongly absorbed; therefore, the first one or two passes inside the needle may determine the final reflectance and transmittance of the ray, while the remaining passes of the ray play a marginal role. However, if the ray is weakly absorbed, it needs more time to decay to such a degree that the remaining passes can be neglected, resulting in potential biases of measured reflectance and transmittance relative to the defined reference due to an improper reference plane used by Daughtry's method. Mutual shadowing between needles was found to be insignificant in reducing the accuracy of Daughtry's method. This conclusion needs to be verified by experiments in further studies, as in this study the leaf interior is assumed to be homogeneous and radiative scattering is neglected. The transmittance and absorption measured by Daughtry's method are theoretically more accurate than the reflectance (overall—not absolutely—Daughtry's method may produce transmittance with large relative errors in some cases, such as in the region of 400–550 nm, when light is incident on the convex side of semicircular-shaped needles; see Figure 12). Therefore, Daughtry's transmittance and absorption can be used in spectroscopic studies of leaf biochemistry, but they are hard to apply to remote-sensing studies at the canopy scale, in which reflectance is the lead optical property.

The biased reflectance and transmittance may introduce great errors in some measured properties such as needle surface refractive index. As mentioned before, the reflectance of a leaf includes two parts: surface reflection and internal scattering. Daughtry's method uses the surfaces of the sample holder rather than the surfaces of needles as the reference plane to distinguish reflected and transmitted radiation. As a result, some reflected radiation, from needle surfaces or interior or both, are incorrectly regarded as transmitted radiation. Current leaf optical-properties models, such as PROSPECT, use a set of fixed refractive indices to describe the reflection happening at leaf surfaces. The refractive indices were calibrated for broad leaves whose reflectance and transmittance can be measured accurately by integrating spheres without any sample holder, as the leaves are broad enough to cover the sample port of integrating spheres. In this case, the leaf surfaces are acting as the reference plane to identify reflected and transmitted radiation, which is consistent with the definition. Therefore, the biased reflectance and transmittance measured by Daughtry's method are likely to result in unsatisfactory performance of leaf optical models. Some studies, such as by Malenovský *et al.*, (2006), attribute the biased performance of PROSPECT with needles to the model structure developed for broad leaves, without paying sufficient attention to possible biases in measured needle reflectance and transmittance. These studies have thus recalibrated the biochemical and biophysical parameters simulated with their measured biased needle reflectance and transmittance. Actually, such recalibrations could be misleading if the measured needle reflectance and transmittance are biased. Compared with Daughtry's method, Harron's method measures both the reflectance and transmittance of needles with negative errors; therefore its measured absorption is always positively biased, which may lead to pronounced overestimation of leaf biochemical traits.

Both Daughtry's and Harron's methods take the faces of sample holders as the reference plane to distinguish between reflected and transmitted radiation; such sample holders will result in possible biases of measured reflectance and transmittance from convex objects. Therefore, the Gordian knot of accurate measurement of needle reflectance and transmittance may be the design of sample holders that can capture the reflected radiation from a convex needle surface in the forward scattering direction (away from the light source). There may be two viable solutions to cutting the knot. The first one is to design a sample holder for a single needle in an integrating sphere. The needle is placed on a flat supporting surface at the receiving side of the sphere with the following conditions: the area under the needle is black so that it does not reflect transmitted radiation through the needle, and the unshaded supporting surface is 100% white so that the radiation reflected by the needle in the forward direction can be reflected back into the integrating sphere. However, such a measuring system has a rather strict requirement for high sensitivity of the measuring sensor, since a needle is often too narrow to provide sufficient signals for measurement.

The second solution is to use multiple needles in a similar setting to the first solution's, in order to provide enough signals for measurement. With a blackened supporting surface

under each needle and white surfaces between needles, all radiation reflected by the needles in the forward direction can be reflected back to the integrating sphere. However, the radiation reflected by the white surface would interact with the needles and be partly absorbed by the needles. Hence a small reflective ridge may be placed between needles to prevent mutual scattering between them. A practical solution would be to place each needle in a concave trough with width selected to minimize the scattering back to the same needle. Although we have not found a practical solution to this complex issue, we would like to specify the requirements for measuring reflectance from a convex needle surface: the surface should be fully exposed to the incoming radiation, the interfusion of reflected and transmitted radiation on convex needle surfaces should be avoided, and for a holder with multiple needles, multiple scattering among needles should be avoided.

Conclusions

This study demonstrates that the directional-hemispherical reflectance and transmittance of needle-shaped leaves measured by two widely used techniques with integrating spheres can be significantly biased, which is obvious across the whole spectral range for Harron's method and remarkable at spectral regions with weak absorption characteristics for Daughtry's method. This finding is of fundamental importance for diverse research fields where accurate DHR and DHT of needle-shaped leaves are needed. To address this issue, we proposed a definition of needle leaf reflectance and transmittance based on a reference plane which separates the illuminated and shaded sides of needles. We also proposed basic requirements for making measurements of needle reflectance and transmittance using an integrating sphere, including a collimated light source, full exposure of the entire needles to the light source, and exposure of the largest side to the light source. The definition given in this study can serve as a theoretical foundation for the development of new measurement techniques.

Acknowledgments

This research was supported by the National Natural Science Foundation of China (41971304, 41671343, 41371070), the Strategic Priority Research Program of Chinese Academy of Sciences (XDA20060402) and the key research and development program for global change and adaptation (2016YFA0600202). We hereby express our sincere gratitude to Stéphane Jacquemoud of iPGP (Institut de physique du globe de Paris) and Jean-Baptiste Féret and others for providing the source code of PROSPECT-5. We also thank Yongqing Zhang and Holy Croft for providing the black-spruce data set used in this study.

References

Abdullah, H., R. Darvishzadeh, A. K. Skidmore, T. A. Groen and M. Heurich. 2018. European spruce bark beetle (*Ips typographus,* L.) green attack affects foliar reflectance and biochemical properties. *International Journal of Applied Earth Observation and Geoinformation* 64:199–209.

Astrup, R., P. Y. Bernier, H. Genet, D. A. Lutz and R. M. Bright. 2018. A sensible climate solution for the boreal forest. *Nature Climate Change* 8 (1):11–12.

Bousquet, L., S. Lachérade, S. Jacquemoud and I. Moya. 2005. Leaf BRDF measurements and model for specular and diffuse components differentiation. *Remote Sensing of Environment* 98 (2–3):201–211.

Brandt, J. P., M. D. Flannigan, D. G. Maynard, I. D. Thompson and W.J.A. Volney. 2013. An introduction to Canada's boreal zone: Ecosystem processes, health, sustainability, and environmental issues. *Environmental Reviews* 21 (4):207–226.

Chen, J. M. and T. A. Black. 1992. Defining leaf area index for non-flat leaves. *Plant, Cell & Environment* 15 (4):421–429.

Comar, A., F. Baret, F. Viénot, L. Yan and B. de Solan. 2012. Wheat leaf bidirectional reflectance measurements: Description and quantification of the volume, specular and hot-spot scattering features. *Remote Sensing of Environment* 121:26–35.

Croft, H., J. M. Chen, Y. Zhang, A. Simic, T. L. Noland, N. Nesbitt and J. Arabian. 2015. Evaluating leaf chlorophyll content prediction from multispectral remote sensing data within a physically-based modelling framework. *ISPRS Journal of Photogrammetry and Remote Sensing* 102:85–95.

Daughtry, C.S.T., L. L. Biehl and K. J. Ranson. 1989. A new technique to measure the spectral properties of conifer needles. *Remote Sensing of Environment* 27 (1):81–91.

Dawson, T. P., P. J. Curran and S. E. Plummer. 1998. LIBERTY—Modeling the effects of leaf biochemical concentration on reflectance spectra. *Remote Sensing of Environment* 65 (1):50–60.

Féret, J.-B., C. François, G. P. Asner, A. A. Gitelson, R. E. Martin, L.P.R. Bidel, S. L. Ustin, G. le Maire and S. Jacquemoud. 2008. PROSPECT-4 and 5: Advances in the leaf optical properties model separating photosynthetic pigments. *Remote Sensing of Environment* 112 (6):3030–3043.

Féret, J.-B., G. le Maire, S. Jay, D. Berveiller, R. Bendoula, G. Hmimina, A. Cheraiet, J. C. Oliveira, F. J. Ponzoni, T. Solanki, F. de Boissieu, J. Chave, Y. Nouvellon, A. Porcar-Castell, C. Proisy, K. Soudani, J.-P. Gastellu-Etchegorry and M.-J. Lefèvre-Fonollosa. 2019. Estimating leaf mass per area and equivalent water thickness based on leaf optical properties: Potential and limitations of physical modeling and machine learning. *Remote Sensing of Environment* 231:110959.

Ganapol, B. D., L. F. Johnson, P. D. Hammer, C. A. Hlavka and D. L. Peterson. 1998. LEAFMOD: A new within-leaf radiative transfer model. *Remote Sensing of Environment* 63 (2):182–193.

Grant, L., C.S.T. Daughtry and V. C. Vanderbilt. 1993. Polarized and specular reflectance variation with leaf surface features. *Physiologia Plantarum* 88 (1):1–9.

Harron, J. W. 2002. Optical properties of phytoelements in conifers. Master's thesis, York University.

Harron, J. and Miller, J., 2002. An alternate methodology for reflectance and transmittance measurements of conifer needles, *Proceedings of the 17th Canadian Symposium on Remote Sensing*, 1995, Saskatoon, Saskatchewan, Canada, pp. 654-661.

Hosgood, B., S. Jacquemoud, G. Andreoli, J. Verdebout, G. Pedrini and G. Schmuck. 1995. *Leaf Optical Properties Experiment 93 (LOPEX93)*. Catalogue No. CL-NA-16095-EN-C. Luxembourg: Office for Official Publications of the European Communities.

Hovi, A., P. Raitio and M. Rautiainen. 2017. A spectral analysis of 25 boreal tree species. *Silva Fennica* 51 (4):7753.

Jacquemoud, S. and F. Baret. 1990. PROSPECT: A model of leaf optical properties spectra. *Remote Sensing of Environment* 34 (2):75–91.

Jacquemoud, S. and L. Ustin. 2008. Modeling Leaf Optical Properties. <http:// http://photobiology.info/Jacq_Ustin.html> Accessed 25 April 2018.

Jacquez, J. A. and H. F. Kuppenheim. 1955. Theory of the integrating sphere. *Journal of the Optical Society of America* 45 (6):460–470.

Lukeš, P., P. Stenberg, M. Rautiainen, M. Mõttus and K. M. Vanhatalo. 2013. Optical properties of leaves and needles for boreal tree species in Europe. *Remote Sensing Letters* 4 (7):667–676.

MacDicken, K. Ö. Jonsson, L. Piña, L. Marklund, S. Maulo, V. Contessa, Y. Adikari, M. Garzuglia, E. Lindquist, G. Reams and R. D'Annunzio. 2015. *Global Forest Resources Assessment 2015: How Are the World's Forests Changing?*, 2nd ed. Rome, Italy: Food and Agriculture Organization of the United Nations.

Maier, S. W., W. Lüdeker and K. P. Günther. 1999. SLOP: A revised version of the stochastic model for leaf optical properties. *Remote Sensing of Environment* 68 (3):273–280.

Malenovský, Z., J. Albrechtová, Z. Lhotáková, R. Zurita-Milla, J.G.P.W. Clevers, M. E. Schaepman and P. Cudlín. 2006. Applicability of the PROSPECT model for Norway spruce needles. *International Journal of Remote Sensing* 27 (24):5315–5340.

Marín, S.d.T., M. Novák, K. Klanůnik and A. Gaberšůk. 2016. Spectral signatures of conifer needles mainly depend on their physical traits. *Polish Journal of Ecology* 64 (1):1–13.

McClendon, J. H. 1984. The micro-optics of leaves. I. Patterns of reflection from the epidermis. *American Journal of Botany* 71 (10):1391–1397.

Mesarch, M. A., E. A. Walter-Shea, ,G. P. Asner, E. M. Middleton and S. S. Chan. 1999. A revised measurement methodology for conifer needles spectral optical properties: Evaluating the influence of gaps between elements. *Remote Sensing of Environment* 68 (2):177–192.

Middleton, E. M., S. S. Chan, M. A. Mesarch and E. A. Walter-Shea. 1996. A revised measurement methodology for spectral optical properties of conifer needles. Pages 1005–1009 in *IGARSS '96: 1996 International Geoscience and Remote Sensing Symposium*, held in Lincoln, Neb., 27–31 May 1996. Los Alamitos, Calif.: IEEE.

Miller, O. E. and A. J. Sant. 1958. Incomplete integrating sphere. *Journal of the Optical Society of America* 48 (11):828–831.

Moorthy, I., J. R. Miller and T. L. Noland. 2008. Estimating chlorophyll concentration in conifer needles with hyperspectral data: An assessment at the needle and canopy level. *Remote Sensing of Environment* 112 (6):2824–2838.

Mõttus, M., A. Hovi and M. Rautiainen. 2017. Theoretical algorithm and application of a double-integrating sphere system for measuring leaf transmittance and reflectance spectra. *Applied Optics* 56 (3):563–571.

Noda, H. M., T. Motohka, K. Murakami, H. Muraoka and K. N. Nasahara. 2013. Accurate measurement of optical properties of narrow leaves and conifer needles with a typical integrating sphere and spectroradiometer. *Plant, Cell & Environment* 36 (10):1903–1909.

Olascoaga, B., A. Mac Arthur, J. Atherton and A. Porcar-Castell. 2016. A comparison of methods to estimate photosynthetic light absorption in leaves with contrasting morphology. *Tree Physiology* 36 (3):368–379.

Pickering, J. W., C.J.M. Moes, H.J.C.M. Sterenborg, S. A. Prahl and M.J.C. van Gemert. 1992. Two integrating spheres with an intervening scattering sample. *Journal of the Optical Society of America A* 9 (4):621–631.

Pickering, J. W., S. A. Prahl, N. van Wieringen, J. F. Beek, H.J.C.M. Sterenborg and M.J.C. van Gemert. 1993. Double-integrating-sphere system for measuring the optical properties of tissue. *Applied Optics* 32 (4):399–410.

Potůková, M., L. Červená, L. Kupková, Z. Lhotáková, P. Lukeš, J. Hanuš, J. Novotný and J. Albrechtová. 2016. Comparison of reflectance measurements acquired with a contact probe and an integration sphere: Implications for the spectral properties of vegetation at a leaf level. *Sensors* 16 (11):1801.

Qiu, F., J. M. Chen, W. Ju, J. Wang, Q. Zhang and M. Fang. 2018. Improving the PROSPECT model to consider anisotropic scattering of leaf internal materials and its use for retrieving leaf biomass in fresh leaves. *IEEE Transactions on Geoscience and Remote Sensing* 56 (6):3119–3136.

Rajewicz, P. A., J. Atherton, L. Alonso and A. Porcar-Castell. 2019. Leaf-level spectral fluorescence measurements: Comparing methodologies for broadleaves and needles. *Remote Sensing* 11 (5):532.

Schaepman-Strub, G., M. E. Schaepman, T. H. Painter, S. Dangel and J. V. Martonchik. 2006. Reflectance quantities in optical remote sensing—definitions and case studies. *Remote Sensing of Environment* 103 (1):27–42.

Wang, B. J. and W. Ju. 2017. Limitations and improvements of the leaf optical properties model Leaf Incorporating Biochemistry Exhibiting Reflectance and Transmittance Yields (LIBERTY). *Remote Sensing* 9 (5):431.

Yáñez-Rausell, L., M. E. Schaepman, J.G.P.W. Clevers and Z. Malenovský. 2014. Minimizing measurement uncertainties of coniferous needle-leaf optical properties, part I: Methodological review. *IEEE Journal of Selected Topics in Applied Earth Observations and Remote Sensing* 7 (2):399–405.

Zarco-Tejada, P. J., J. R. Miller, J. Harron, B. Hu, T. L. Noland, N. Goel, G. H. Mohammed and P. Sampson. 2004. Needle chlorophyll content estimation through model inversion using hyperspectral data from boreal conifer forest canopies. *Remote Sensing of Environment* 89 (2):189–199.

Zhang, Y., J. M. Chen, J. R. Miller and T. L. Noland. 2008a. Leaf chlorophyll content retrieval from airborne hyperspectral remote sensing imagery. *Remote Sensing of Environment* 112 (7):3234–3247.

Zhang, Y., J. M. Chen, J. R. Miller and T. L. Noland. 2008b. Retrieving chlorophyll content in conifer needles from hyperspectral measurements. *Canadian Journal of Remote Sensing* 34 (3):296–310.